Pressure Evolution of Laser-Induced

Cavitations and Shock Waves

A thesis submitted in partial fulfillment of the requirement for the degree of Bachelor of Sciences with Honors in Physics
from the College of William and Mary in Virginia,

by

Brian Robert Koch

Accepted for _____
Honors

William E. Cooke_____
Advisor

Gina L. Hoatson_____

Kenneth G. Petzinger_____

Margaret S. Saha_____

Williamsburg, Virginia
May 2003

Abstract

Using various optical imaging techniques, we have obtained values for the pressures of cavitations and their shock waves for times between 5 nanoseconds and 30 microseconds after the origination of the cavitation. We induced cavitations in various liquids by a pulsed, frequency doubled Neodymium-Yttrium-Aluminum Garnet (Nd:YAG) laser (532 nm), or a dye laser (560 nm) pumped by this Nd:YAG laser. For times between 1 and 30 microseconds, we imaged the cavitations onto a CCD camera using an electronic delay box, which delayed a dye laser from the Nd: YAG laser. For times between 5 and 45 nanoseconds, we used two optically delayed dye lasers to image onto a color, digital camera. By comparing the radii of the cavitations or shock waves from different times, we determined the pressure at different times after the cavitation's initial formation. We found that the pressure is greatest initially, within the first 5 ns.

We have also obtained data to determine the probability of a cavitation event under various conditions. To do this we used a counting circuit to take data on the number of cavitations per unit time for varying liquids, focal length focusing lens, and laser powers. As expected, we found that a tighter focus and higher laser power induce more explosions.

1. Introduction

The primary goal of this project is to obtain an accurate description of how the pressure evolves from 5 ns to 45 ns following laser-induced cavitation formation. Combining this with our previous data, we have a general description of cavitation pressure and shock wave pressure from 5 ns to 30 microseconds. Our eventual goal is to

be able to induce single cavitations and to know the resulting pressure and temperature as a function of time and as a function of distance from the origin. These temperature and pressure gradients are expected to be useful in inducing biological processes. Some possibilities are fusing liposomes or vesicles together or optoporation, using pressure waves from the cavitations.

A laser-induced cavitation is a formation of gas and plasma in a liquid caused by a focused, pulsed laser beam. The laser beam passes through a microscope lens that focuses the beam into a small cuvette made of thin plastic containing a liquid (see Figure 1). Energy is deposited at the focus of the laser beam, leading to an explosion that results in a cavitation that expands with time.

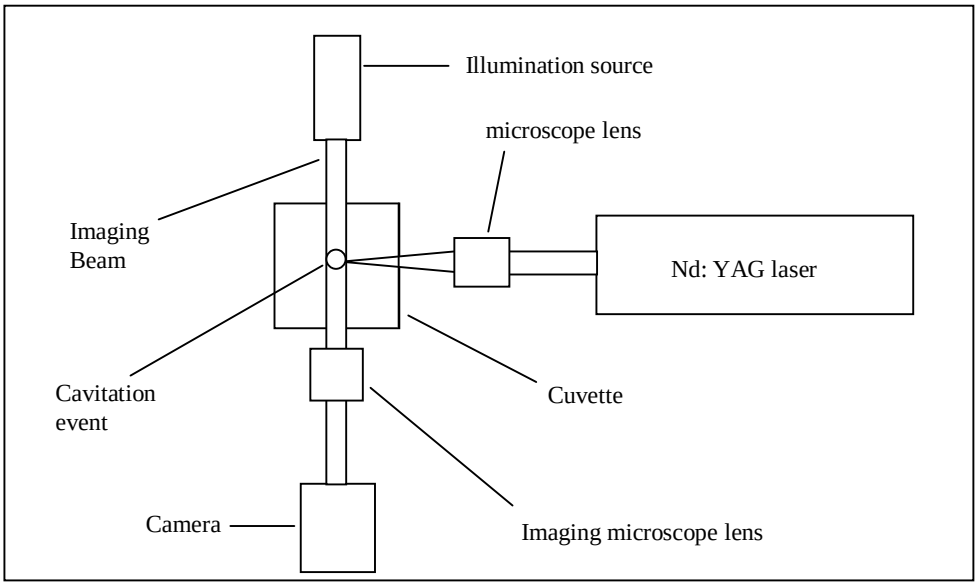

Figure 1 - Simplified experimental setup, viewed from above. The Nd: YAG beam is focused by the microscope lens to induce cavitations. The illuminating beam(s) pass through lenses from the orthogonal direction, into the cuvette and through an imaging microscope lens to form an image on the video camera.

Cavitations have been studied considerably in the past for a variety of reasons. Most recent studies have focused on the collapse of cavitations, either to initiate sonoluminescence [1], or as a primary cause of erosion [2]. However, there have been studies on the distribution of the laser energy in a cavitation [3, 4] and pressures of cavitations at different times after initiation as part of a program to develop better forms of laser eye surgery [4]. Results of these experiments show that the conversion of absorbed laser energy to mechanical energy is about 90% for nanosecond laser pulses using large focusing angles and high pulse energy (22 degree focusing angle and 1 or 10 mJ laser pulse energy). This mechanical energy decreases with shorter pulses, smaller focusing angle (weaker focus), or less pulse energy. These experiments also show that cavitation pressure is highest initially, and decreases rapidly. In our experiments, we tested the effect of the focusing angle and laser energy, using a constant pulse duration of 2 ns.

In the summer of 2001 Brett Jacobs et al [5] observed strong enhancement of cavitations at low pulse energies when initiated in an oil droplet. This led us to investigate the effects of various objects suspended in liquids. We tested the effects of 10 micron polystyrene micro-spheres and 0.7 micron quartz micro-spheres suspended in water as compared to distilled water.

Other studies have investigated the use of cavitations to inject drugs into cells [6]. They claim that efficient cavitation-driven drug delivery can be achieved with little or no damage to normal tissues. If this is possible, it may be possible to deliver other chemicals to individual cells without damaging the cell or to join liposomes without

damaging them. We have begun to investigate this application by examining cell death rates for cells exposed to laser-induced cavitations.

2. Calibration and Beam Profiles

2.1 Calibration of the System (Magnification)

Accurate calibration of our setup is essential to all aspects of this study. Since all of our experiments require the use of a video camera to view events, we need to know the size of the objects in our images. Calibrating the system requires converting the number of pixels in our captured images to an actual distance.

To determine our calibration, we placed a cuvette containing 10 micron spheres in the beam like those in Figure 2a. By imaging the spheres, we can determine the number of pixels taken up by each sphere. Knowing the size of the spheres then allows us to know how many microns are in each pixel.

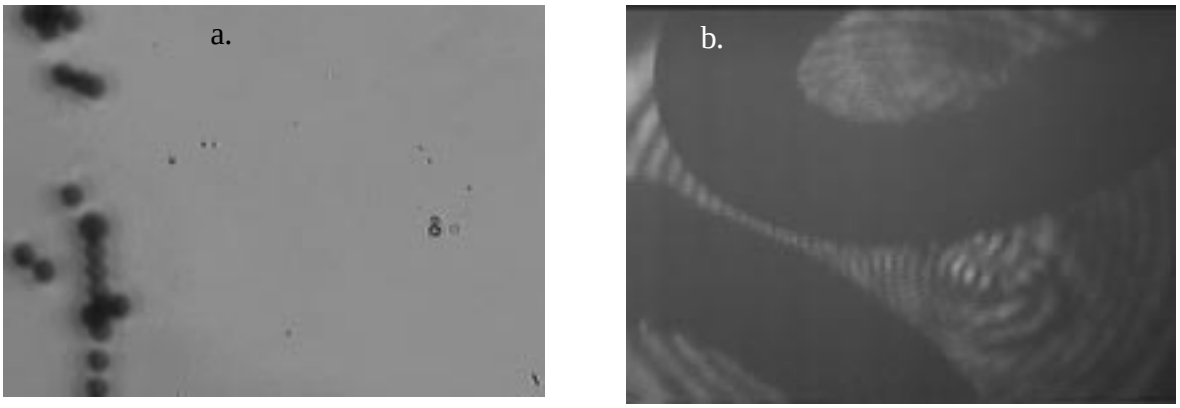

Figure 2 – Calibration techniques. (a) 10 micron spheres. The spheres are imaged onto the camera. Knowing the size of the sphere easily allows us to determine how many microns each pixel on the camera screen takes up. (b) In order to obtain more accurate results, larger objects can be used such as a wire.

The magnification was different for each of our experiments, but we give the following calculations as an example calibration. We found that a 10 micron sphere (in focus) took up 18±2 pixels on the computer screen, so that each pixel corresponds to 0.56 ± 0.06 microns. We also repeated these measurements using a wire of known thickness and obtained the same calibration (Figure 2b). Using the wire we could also measure the pixel aspect ratio (size in the vertical direction as compared to that in the horizontal direction). The aspect ratio is easily determined by rotating the camera by 90 degrees and measuring again. In later experiments we changed the distance of the camera to obtain greater magnification and therefore our calibration changed (details are given where needed). Other methods for performing a more accurate calibration are being investigated.

2.2 Beam Profile Measurement

In order to fully understand how cavitations occur, we need to know the exact profile of our cavitation-inducing beam. To do this we carefully lined up the laser and passed it through the microscope lens. We examined the shape of the beam on a screen placed some distance away from the microscope lens. We expect the shape to be circular. We examined how this shape changed when neutral density filters of known values were used to attenuate the intensity incrementally. Using this method, we examined the profile of a yellow dye laser laser (560 nm) pumped by the Nd: YAG laser, and found that the focus was nearly a diffraction limited Gaussian spot. This laser was used in all of the count rate data.

Another method was used to measure the beam profile of the Nd: YAG laser (used to induce cavitations in all other experiments). The laser beam was aimed into the

cuvette through a microscope lens and the camera was set up to view the cuvette from the side, as in the normal setup. The cuvette contained water with 0.7 micron quartz spheres suspended in it. The laser power was turned down enough so that no cavitations were induced. However, the laser light was bright enough to scatter off of the micro-spheres and onto the camera.

Therefore each picture contained light scattered off of several micro-spheres that were in the beam path as shown in Figure 3. Combining multiple pictures and averaging the result (done by a computer program of our own design), effectively shows the distribution of the laser's intensity as a function of vertical position. By taking a vertical section of this picture and analyzing the intensity as it varies with vertical position (again using our computer program), one can get an accurate description of the beam profile. This analysis is currently being completed for the Nd: YAG beam.

Figure 3 - Beam waist and profile as seen from the side. Light from the laser at low power is scattered off of 0.7 micron quartz spheres indicating the intensity of the laser in different regions. It is easy to see where the laser beam converges to its focus on the left end of the picture.

3. Count Rate Studies

3.1 Theory

An important aspect of our study is predicting and controlling cavitations. The goal is to be able to determine what type of cavitation (energy, pressure, size, etc.) will occur for a given laser energy and focal length. Previous experiments have studied the influence of laser pulse duration and focusing angle on the distribution of energy in a cavitation [3]. We investigated how the likelihood of a cavitation occurring changes under different conditions. To study this we have designed and constructed a circuit that counts the number of cavitations in time. We used this counting circuit to take data for different laser powers, focus, and liquids which will tell us the probability of a cavitation occurring at a certain laser power and focus. We expect the count rate to increase with power and tighter focus because of a greater intensity over the laser focus area. We also expect the count rate to increase with objects suspended in the.

3.2 Experimental Methods

To quickly collect data concerning the number of explosions in time for different conditions, we constructed the counting circuit shown in Figures 4-8. The circuit uses a photodiode placed in front of the camera's position (Figure 4). The photodiode creates a voltage whenever a light pulse enters it. Since the explosions emit light, if we aim this light onto the photodiode using a lens, each explosion creates a voltage pulse. This voltage pulse must pass through a fairly complicated circuit to create a pulse that can be counted. The circuit involves a voltage amplifier that eliminates the DC offset of the photodiode, so that only explosions produce a voltage (Figure 5). The next major

component is a one shot set up as shown in Figure 6. This turns the voltage pulses into a standard 5 Volt pulse of appropriate width (time duration). These pulses then feed into a counting chip, with its outputs tied to logic lights, allowing us to view the number of explosions (Figure 7).

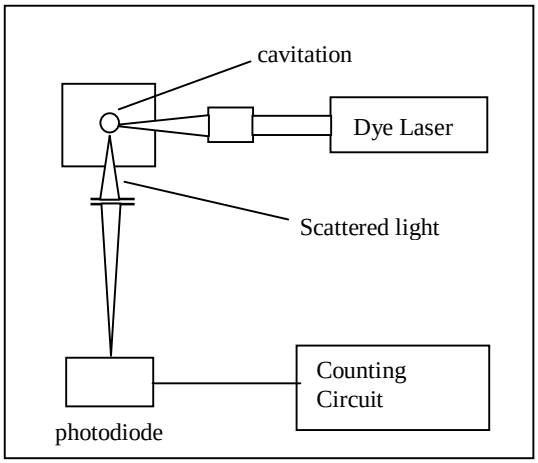

Figure 4 - Counting circuit setup. The cavitations emit light that is aimed into a lens, which then projects the light onto the photodiode.

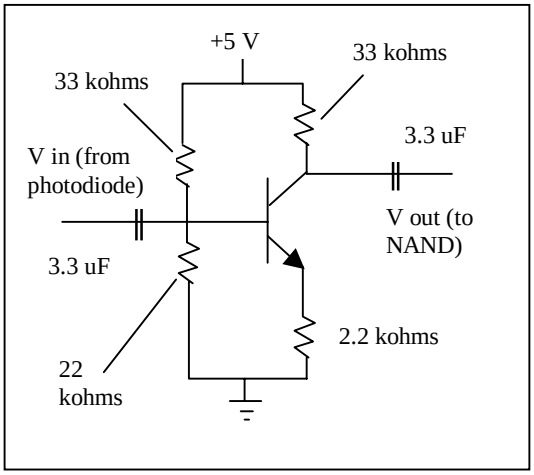

Figure 5 - Voltage amplifier. The output of the photodiode must first be passed through a voltage amplifier in order to eliminate the DC offset. After passing through a NAND gate to invert this output, the output goes to a one shot.

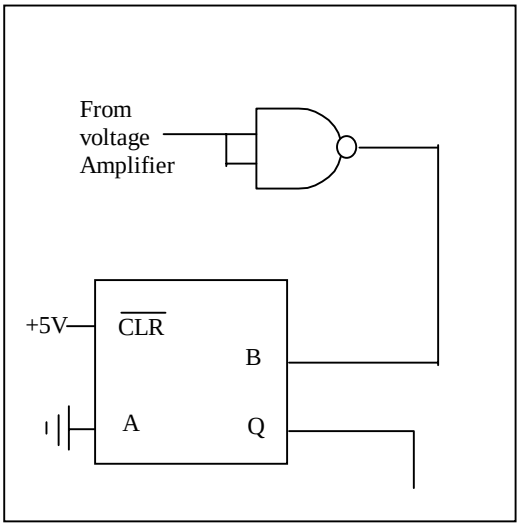

Figure 6 - The one shot creates a pulse of the correct shape to enter the explosion counter. The NAND gate is required here to invert the pulse coming from the voltage amplifier.

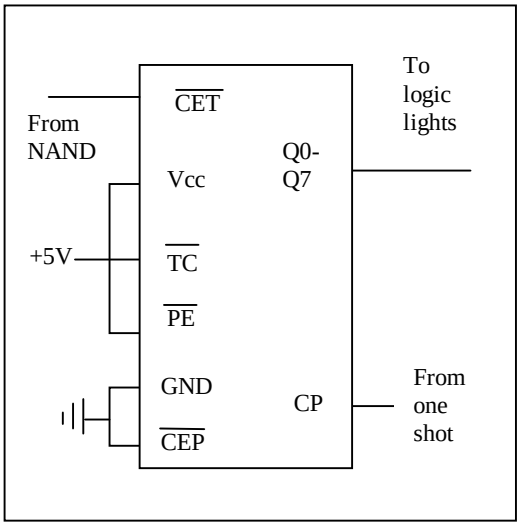

Figure 7 - The explosion counter (counter 1) counts the number of actual cavitations in time (stops after 256 laser pulses). It begins counting when the debounced button is pressed on the circuit board, which tells the counter to begin counting. The number of explosions appears on the logic lights on the circuit board.

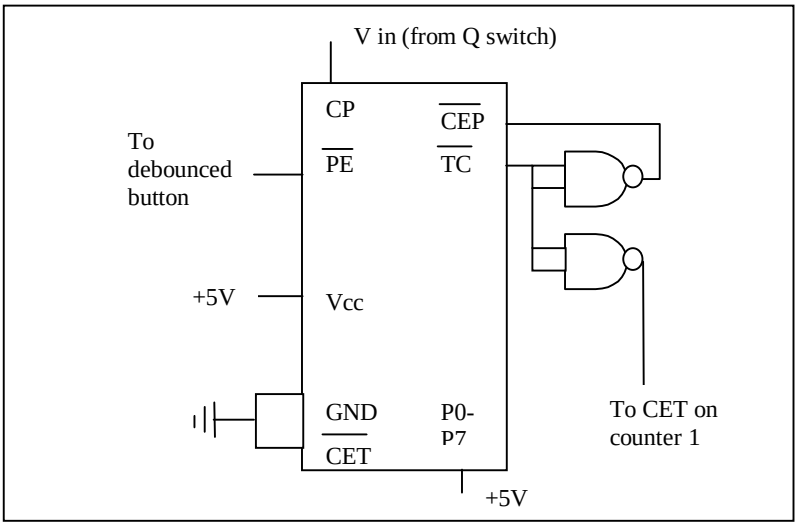

Figure 8 - Timing counter. This circuit takes the number of laser pulses total from the Q-switch on the Nd: YAG laser and stops the explosion counter from counting

The second counter counts the pulses from the Q-switch output of the laser, as shown in Figure 8. This circuit counts 256 laser pulses and then inhibits the other counter. So the circuit counts the number of explosions per 256 laser pulses.

3.3 Measurement of Spot Size

In our analysis of explosions as a function of time for the different focal lengths, we needed to know the spot size (the radius of the beam at the focus) for the two different focal lengths. To do this we again looked at water with 0.7 micron quartz spheres suspended in it. We could clearly see where the focus was because light strongly reflected off of the micro-spheres, as is shown previously in Figure 3.

3.4 Data and Analysis

For all count rate data, a yellow dye laser (560 nm) pumped by the Nd: YAG laser was used to induce cavitations. Our initial studies with the various counting procedures generally agreed with our expectations, but also showed that there were other factors

affecting the count rate. As expected, we found that in general the count increased with increased laser power, a tighter focus (shorter focal length), and liquids with more objects in them (for example, 10 micron polystyrene spheres in water or 0.7 micron quartz spheres in water as opposed to distilled water). As an example, see Table 1 for the dependence on laser power.

Energy versus Probability

Energy (μJ)	1.42	1.13	0.1	0.93	0.89	0.85	0.81	0.77	0.73	0.69	0.64
Count Rate (per 256)	256	232	170	137	91	68	51	37	36	18	6
Count Error	16	15.23	13.04	11.70	9.54	8.25	7.14	6.08	6.00	4.24	2.45
Probability	1	0.906	0.664	0.535	0.355	0.266	0.199	0.145	0.141	0.070	0.023
Prob. Error	0.063	0.059	0.051	0.046	0.037	0.032	0.028	0.024	0.023	0.017	0.010

Table 1 – The energy per pulse (as measured from a power meter placed in the position of the cuvette) versus count rate and probability. Clearly, the count rate decreases with decreasing laser power. For this data the laser frequency was 10 Hz, the liquid was water containing 10 micron spheres, and a 20 micron spot size. The error in the count rate was found by taking the square root of the count rate since this data is based on events. The probability was obtained by dividing the count rate by 256, and the error in the probability was found by dividing the count rate error by 256.

Figures 9 and 10 show the probability of a cavitation occurring versus laser pulse energy for two different liquids and for two different focusing lenses. One can clearly see that water containing 10 micron polystyrene spheres is much more likely to have a cavitation than distilled water under the same conditions. In other words, for a given laser energy, the probability of having a cavitation is considerably higher (20 to 30 percent) in water with micro-spheres than in distilled water. It is also important to note that the threshold energy for a cavitation (the minimum energy required to induce a

cavitation) is lowered by having 10 micron spheres in the water. A tighter focus also reduces the required energy to obtain a given explosion probability.

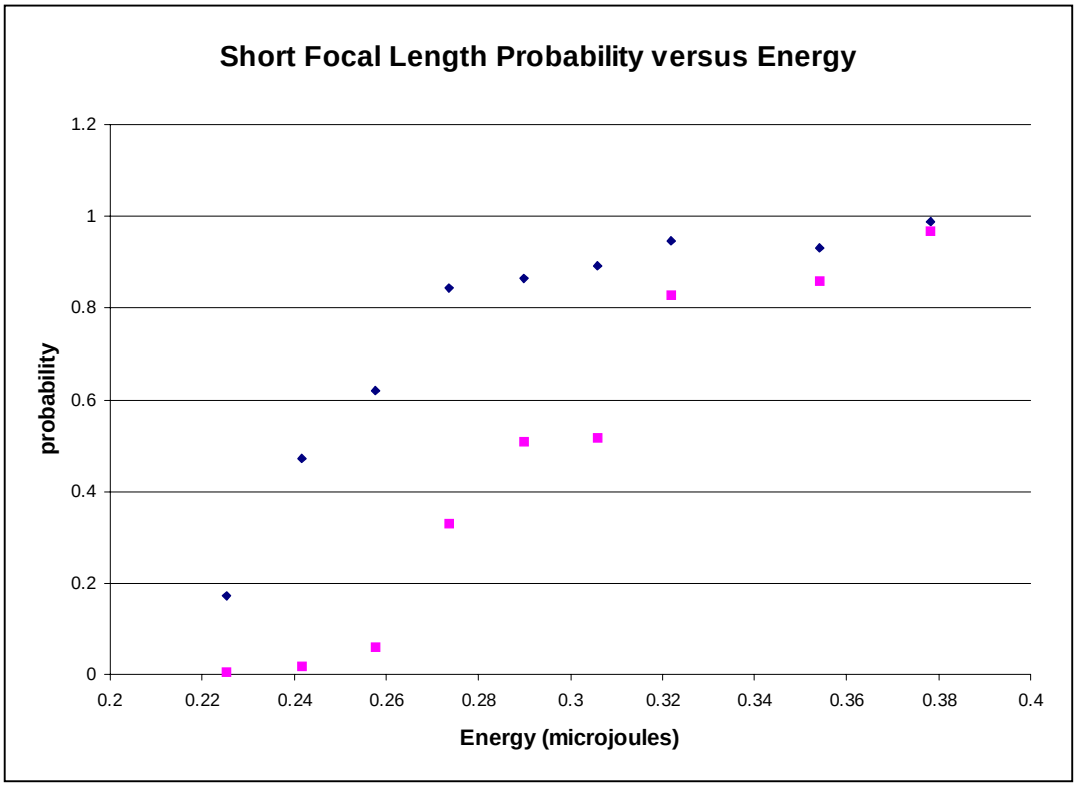

Figure 9 - Probability of a cavitation versus pulse energy for distilled water (pink) and water containing 10 micron spheres (purple) laser frequency 10 Hz. Spot size 10 microns.

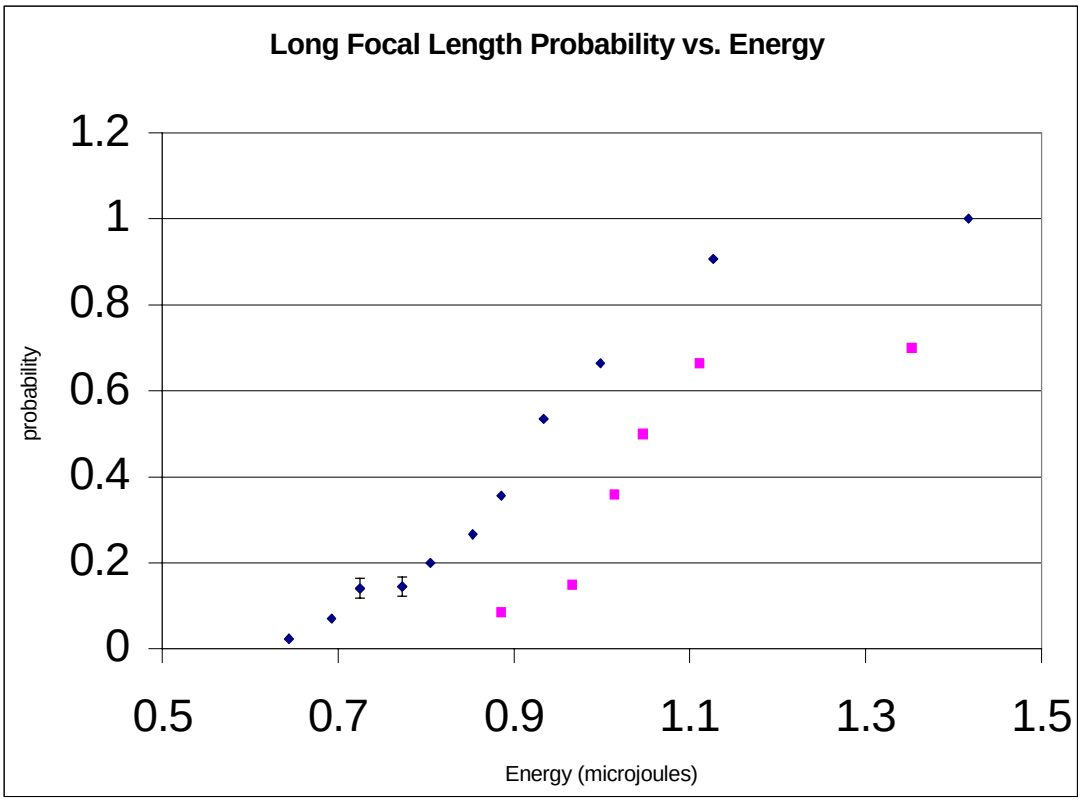

Figure 10 - Probability of a cavitation versus pulse energy for distilled water (pink) and water containing 10 micron spheres (purple) laser frequency 10 Hz.Spot size 20 microns. Notice that the energy required to induce cavitations is much smaller for the 10 micron spot size lens than for the 20 micron spot size lens.

However, we also found that the count rate for water varied with the amount of time after initial laser beam firing and with the exact placement of the cuvette with respect to the laser beam focus. In general the count rate decreased with increasing exposure to the laser beam. Table 2 clearly shows these results. The change in count rate due to placement of the cuvette was completely unpredictable. These results were not found for water with 10 micron polystyrene spheres or water with 0.7 micron quartz

spheres. For these samples, the count rate did not vary with exposure time to the laser beam or placement of the cuvette.

Probability versus Time

Time of Count Rate Start (min:sec)	0	1:40	2:50	3:50	4:35	6:20	8:35	12:15	15:05
Count Rate (per 256)	119	102	76	69	67	61	42	11	14
Count Rate Error	10.91	10.10	8.78	8.31	8.19	7.81	6.48	3.32	3.74
Probability	0.465	0.398	0.297	0.270	0.262	0.238	0.164	0.043	0.055
Prob. Error	0.043	0.039	0.034	0.032	0.032	0.031	0.025	0.013	0.015

Table 2 - The count rate versus time for distilled water, 20 micron spot size, 10 Hz laser pulses. As time progresses the count rate decreases and eventually levels out at a steady slow rate.

We have not found the cause of the change in probability of cavitations with exposure time in water. However, we believe thermal lensing may be occurring. This would cause a defocusing of the laser beam leading to a decreased light intensity in the region near where the cavitations initiate. This would result in fewer cavitations.

4. Pressure Studies from 1 to 30 microseconds

4.1 Theory

The theory behind the conversion of a cavitation radius to a pressure is as follows. We start by assuming that the liquid in the cuvette is incompressible (i.e. ρ=constant). Next we use conservation of mass:

$$\vec{\nabla} \cdot \vec{u} = 0, \qquad (1)$$

in which u is the velocity field. In spherical coordinates, this is

$$\frac{\partial}{\partial r}\left(r^2 u\right) = 0\,. \tag{2}$$

Assuming there is no mass loss into the bubble from the liquid, we have

$$u = \dot{R}\left(\frac{R}{r}\right)^2, \tag{3}$$

in which R is the actual bubble radius. The final assumption is that our cavitations are spherically symmetric. In that case, Newton's Law becomes

$$\frac{1}{\rho}\frac{\partial P}{\partial r} = \frac{du}{dt} = \frac{\partial u}{\partial t} + \left(\vec{u}\cdot\vec{\nabla}\right)u = \frac{\partial u}{\partial t} + u\frac{\partial u}{\partial r}\,. \tag{4}$$

After manipulating these equations, we end up with the equation

$$\Delta P = 40 \times \frac{\left[\frac{d^2}{dt^2}\left(R^{5/2}\right)\right]}{R^{1/2}}, \tag{5}$$

with △P in atmospheres, t in seconds, and R in units of 100 microns.

4.2 Experimental Setup

To study the cavitations between times of 1 and 30 microseconds, we used a dye laser pumped by the Nd: YAG cavitation-inducing laser. The Nd: YAG pump beam is frequency doubled to 532 nm and has a 2 ns pulse duration, with a repetition rate of 10 Hz. The dye beam is delayed from the pump beam using an electronic delay box. The dye beam is light orange and has a pulse duration of about 1 nanosecond. This short pulse duration is desirable in order to obtain sharp images. We also use a diode laser timed with the Nd: YAG to image the cavitations at different times after initiation. Using a computer program (SCION image viewer), we measured the radii of these bubbles at

different times. From this we could determine the pressures inside these bubbles using the equations described above.

All of our reliable data came from measurements made using both the diode laser and a dye laser to image the cavitations. To have both beams reach the cavitation with a similar intensity, we place a glass microscope slide in front of the diode laser at an angle. This slide allows almost all of the diode light to pass through, while also reflecting a small amount of the dye laser light (which comes in at an angle) into the cuvette. Since the original dye laser beam is much more intense than the diode laser, the reflected part of the dye beam has an intensity comparable to that of the diode beam. A typical image is shown in Figure 11.

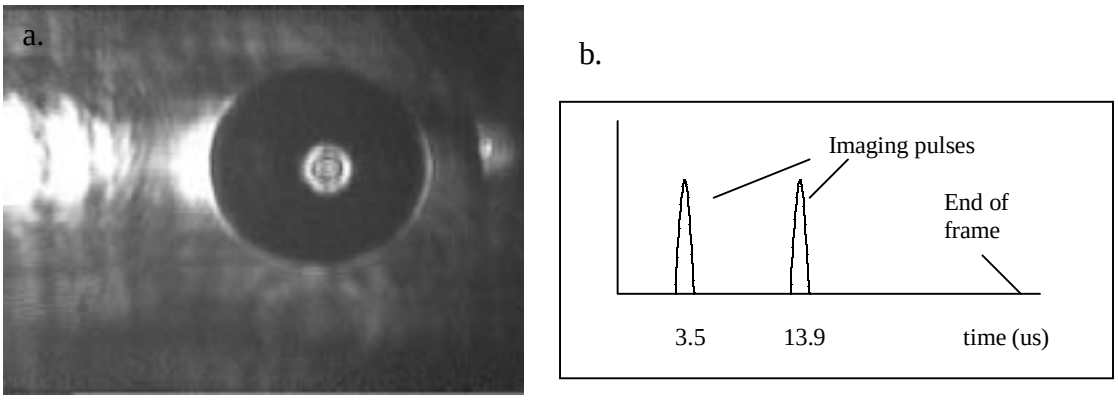

Figure 11 – A dye pulse followed by a diode laser pulse. The dye laser pulse is at 3.5 μs and diode pulse (right) at 13.9 μs. (a) The resulting image. (b) The time layout of the image. Both images occur on the same frame because the frame does not end until much after both pulses have occurred.

Each image has essentially two discs—one for each laser's pulse. The inner disc corresponds to the cavitation at the earlier time, and the outer ring corresponds to the cavitation at the later time. Both appear on the same frame because the pulses are relatively close together in time with respect to the rep rate of the CCD camera (30 Hz).

Only part of the cavitation corresponding to the later time (diode laser pulse) appears on the screen. This is because in order to have the light intense enough to view an edge, the diode beam had to be focused to a small area. However, we know where the center of the cavitation is because of the dye laser's image, so we can still calculate the radius at the time of the diode laser's pulse.

4.3 Diode Laser Circuit Design

The diode laser circuit (triggered on the Nd: Yag laser) involves one-shots to create the correct delay and pulse duration. When the pulse from the trigger goes into the circuit, the one shot waits a certain amount of time (the desired delay time) and then lets out a pulse of the desired width (the pulse duration). The single pulse circuit only requires 2 one shots (one for delay time and one for pulse duration). Changing resistors and capacitors in the one shots can independently change the pulse's delay time and pulse duration.

However, the current coming out of a one shot is very small. To power the diode laser, this current needs to be amplified; this is done using the circuit in Figure 12.

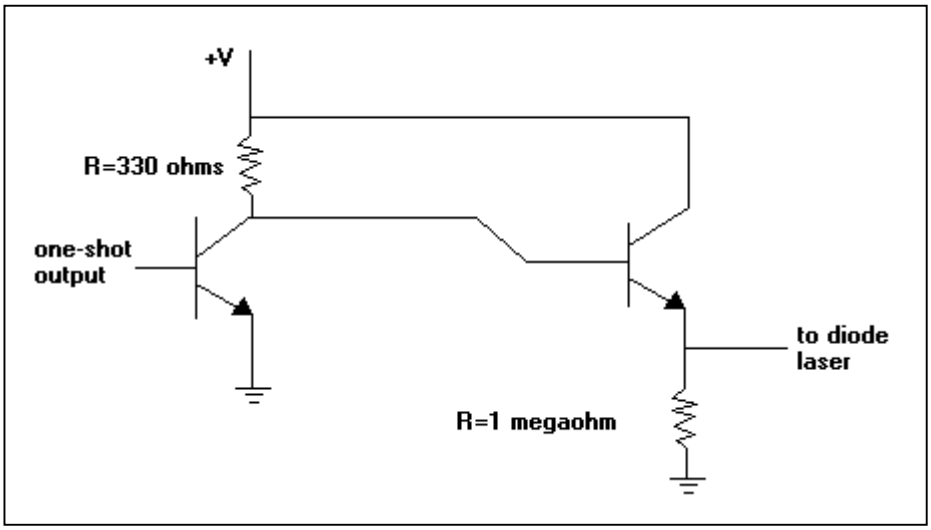

Figure 12 – Diode laser Circuit Design. The output of the one shot (which delays the diode laser pulses from the Nd: YAG cavitation inducing beam and determines the duration of the diode pulses) enters a current amplifier circuit. By adjusting the input voltage (+V) to this circuit, we can change the current that goes to the diode laser. All transistors shown throughout this paper are 2N3904 transistors.

Adjusting the variable voltage into this circuit changes the current coming out of the circuit. This current then goes to the laser. Increasing the current to the laser increases the power output by the laser. So the intensity of the laser beam can be adjusted by adjusting the voltage into the circuit. For illuminating the cavitations, we want the shortest pulse we can see on camera. If the pulses are too long the images get blurred, because the bubble actually grows during the laser pulse. The best pulse length we found seemed to be 0.2 microseconds (which had a power of about 10 mW)

4.4 Data and Analysis

We obtained the cavitation radii directly from the images captured. Using a computer program, we measured the positions of the edges of the cavitation and

subtracted to get the diameter. Dividing by two we obtained the radius. For a given laser power and time delay, the cavitation size can vary significantly, as shown in Figure 13.

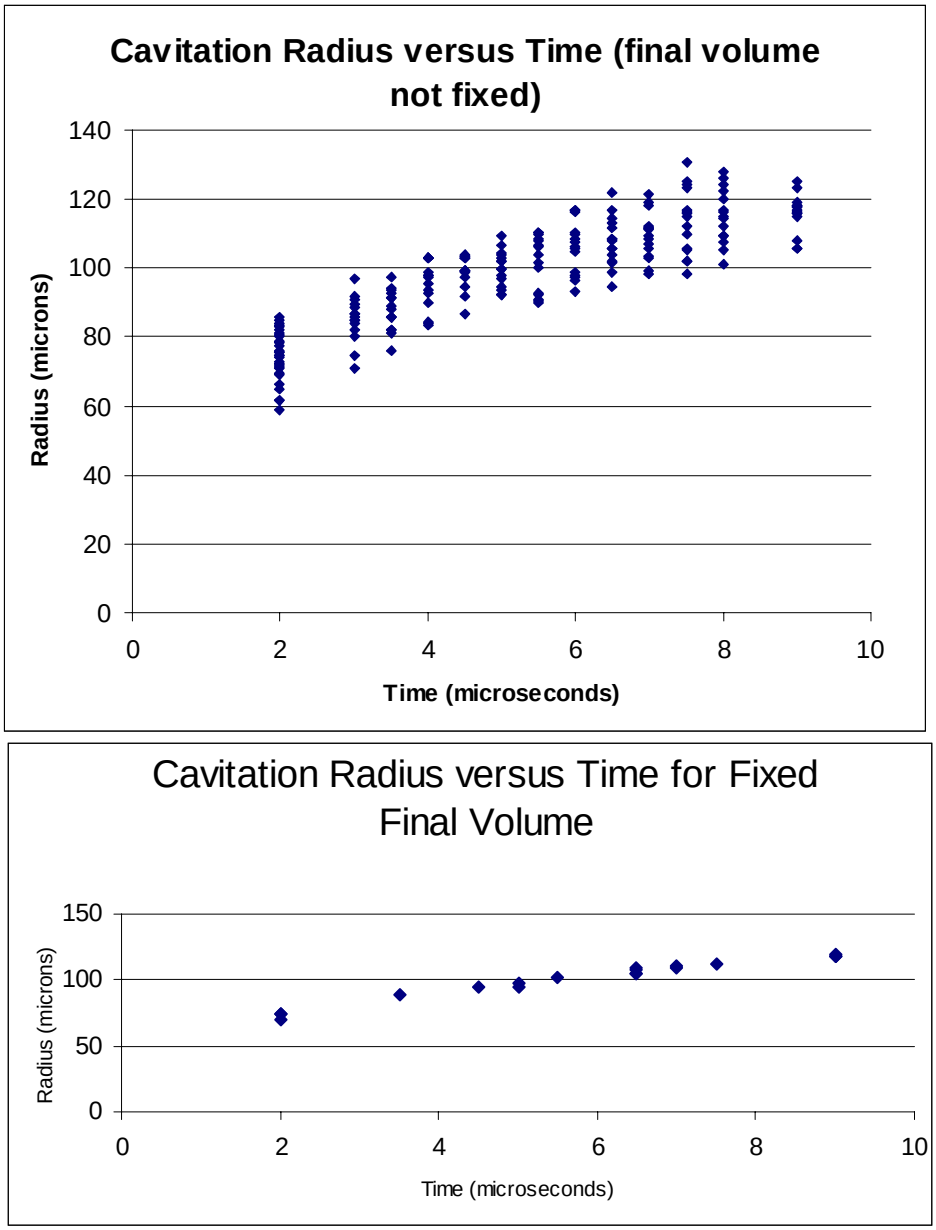

Figure 13 – Cavitation radius versus time. (a) The cavitation size varies considerably (about 30 microns) for a given laser power and time. This fact makes it necessary to use special techniques to compare images of different cavitations. (b) If we observe cavitation radius versus time for cavitations having the same volume at a specific time, there is much less scatter.

Since our data from different time delays are from different cavitation events, we developed a simple method to treat different cavitations as the same cavitation. We observed many cavitations with delays of 5 microseconds and another delay at a variety of later times. We determined from this information that if 2 different cavitations had the same radius at 5 microseconds then their radii at the later time were the same within a 5% margin of error. Therefore we can treat these separate cavitations as the same cavitation in our analysis. This same process was tested for a fixed delay at 13.9 microseconds used with a variable delay covering earlier and later times. Again, different cavitations with the same radius at 13.9 seconds had very similar radii at earlier and later times.

From our diode/dye data, we found that bubble size (volume) increases until about 20 microseconds (see Figure 14), when it begins to shrink back down. We plotted

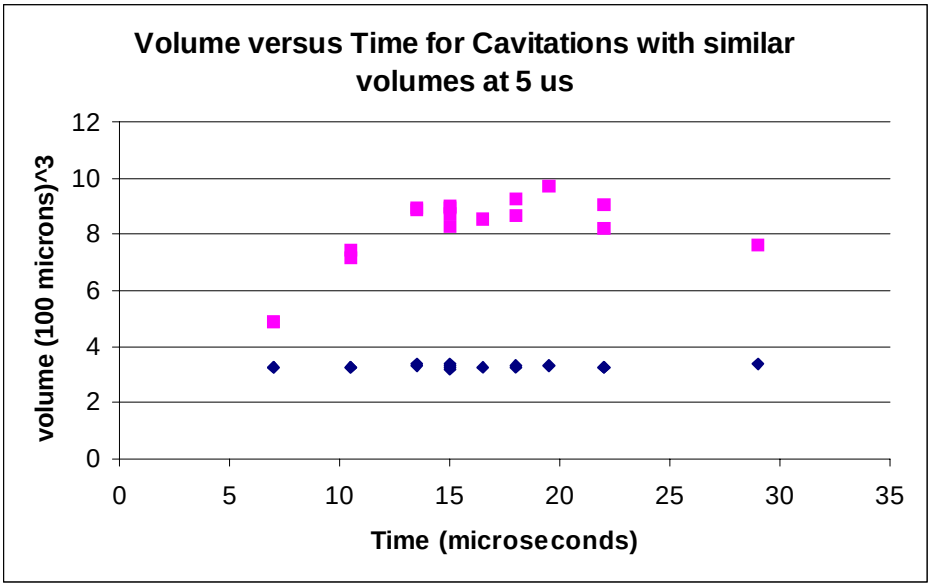

Figure 14 – Volume versus time for cavitations with similar 5 microsecond volumes. The purple points indicate the volume the cavitation had at 5 microseconds for the corresponding second pulse at the time on the x axis. The pink points are the volumes of the cavitations at the variable second delay time. Since the 5 microsecond volumes make a straight line, the pink points can be treated as the same cavitation.

volume instead of radius, because our cavitations are elliptical, and not spherical. Therefore finding the volume and then obtaining an effective $R^{5/2}$ is more accurate than if we just measured the radius in one plane or the other. We obtained the radius by treating the volume calculated as if it were a sphere (divide by $4\pi/3$, and take the cube root of that result). The effective $R^{5/2}$ was obtained from this radius, and plot of $R^{5/2}$ as a function of time is shown in Figure 15. We calculated the pressure from the curvature of this graph, and it is shown in Figure 16.

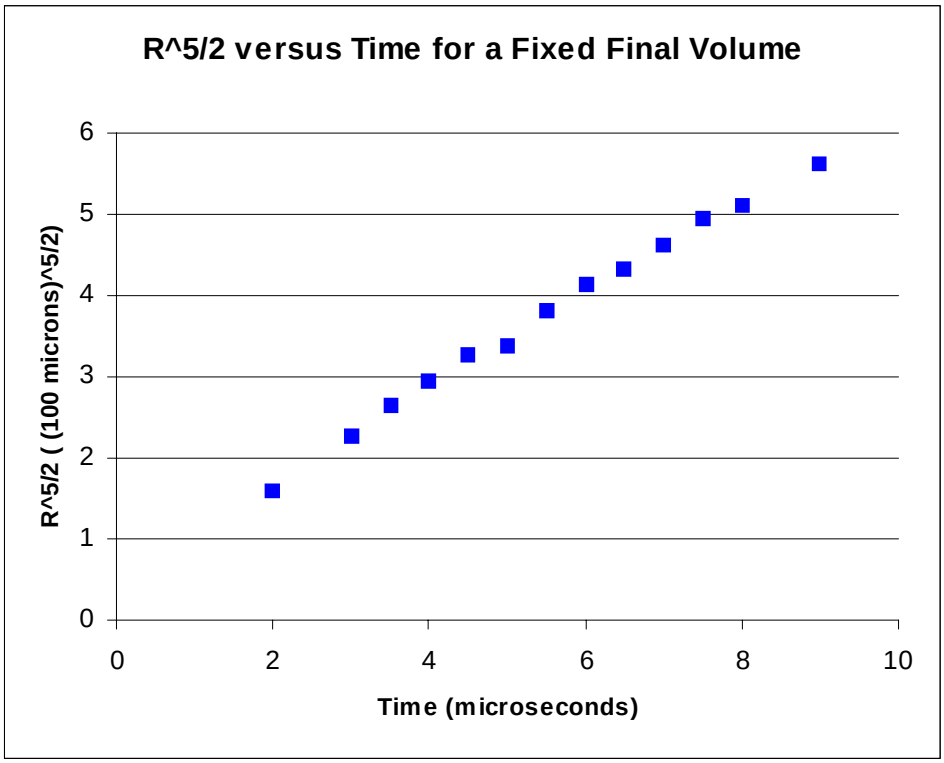

Figure 15 - $R^{5/2}$ versus time for a fixed final volume. All points on this graph can be treated as the same cavitation because their volumes at 13.9 microseconds were the same.

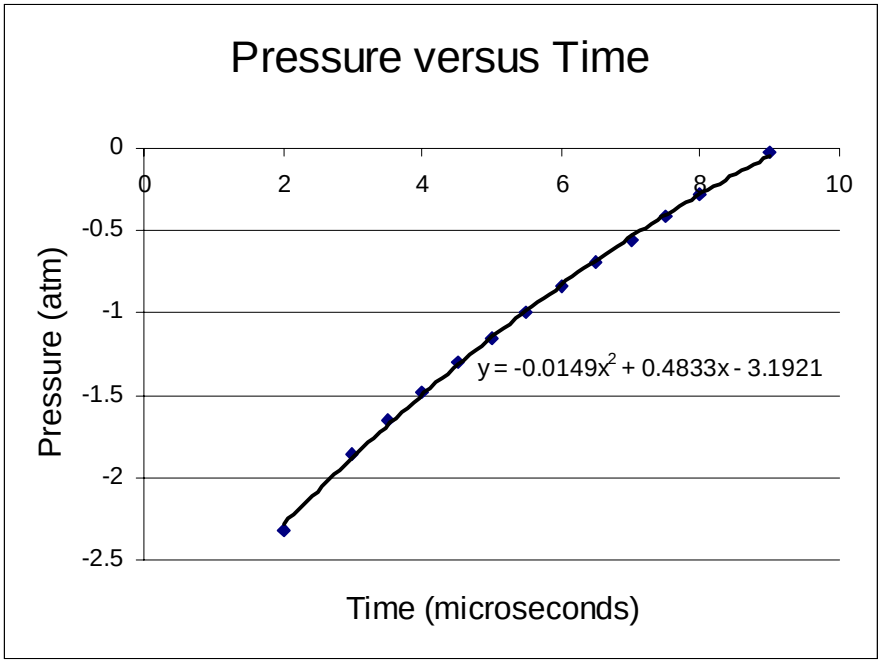

Figure 16 – Pressure versus time for 2 to 10 microseconds. The pressure starts out at a negative value and slowly increases towards 0. In some cases the pressure becomes slightly positive at later times.

The pressure starts out at a negative value (means the pressure is inward on the bubble) and goes towards zero with increasing time (usually passing through 0 to positive pressures eventually). We find that the pressure is most significant at the earliest time, but this is an inward pressure on the bubble. The maximum is near 2.5 atmospheres at 2 microseconds after cavitation formation.

5. Pressure Studies from 5 to 45 nanoseconds

5.1 Theory

Using another model we can determine the pressure resulting from a cavitation's shock wave (rather than from a cavitation itself) based on the shock wave velocity. The pressure is given by the Huginiot Curve found by Rice and Walsh

$$p_s = c_1 \rho_0 u_s \left(10^{(u_s - c_0)/c_2} - 1\right) + p_\infty \tag{6}$$

where c_0 is the normal sound velocity in the liquid (water), c_1=5190 m/s, c_2=25,306 m/s, p_∞= 100000 is the hydrostatic pressure, ρ_0=998, and u_s is the speed of the shock wave [4]. This model is accurate only if the shock wave velocity is significantly larger than the velocity of sound in the liquid. In order to use this method, we must analyze the shock wave radii at times earlier than 50 nanoseconds after initiation.

Another model that can be used to determine shock wave pressure is the Tait equation, which is

$$\mathrm{p_s} = (p_\infty + B)\left(\frac{2nu_s^2}{(n+1)c_0^2} - \frac{n-1}{n+1}\right) - B \tag{7}$$

where c_0 is the normal sound velocity in the liquid (water), p_∞=100000 is the hydrostatic pressure, u_s is the speed of the shock wave, B=314 MPa, and n=7 [4]. This model fits experimental data for pressure values up to 2500 MPa (24673.1 atm) [7]. A comparison of these two models is shown in Figure 17, which shows the pressure as a function of shock wave velocity for the two models. We can see that for speeds near the speed of sound in water (1483 m/s), the models agree. Taking the Taylor's series expansion of each equation about u=1483 m/s, we can also see that they are in close agreement. The Rice and Walsh model gives, to third order

$$100000 + 7\times10^5(u-1483) + 500(u-1483)^2 \quad (8)$$

The Tait model is, to third order

$$100000 + 7.4\times10^5(u-1483) + 250(u-1483)^2 \quad (9)$$

In both cases, the higher order terms are very small.

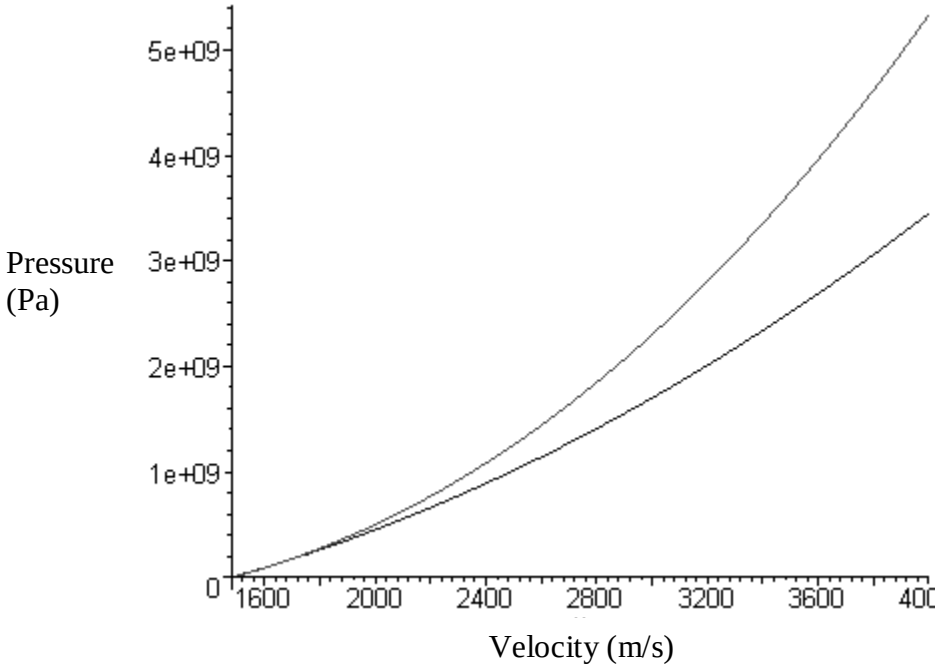

Figure 17 – Pressure versus velocity for two different models. The Rice and Walsh model curve is in red, and the Tait equation is in blue. The Tait equation is accurate only for speeds up to 2500 m/s. At velocities near the speed of sound, the two models are very close.

5.2 Experimental Setup

Using 2 dye laser pulses at different times and with different wavelengths (colors), we obtained 2 rings in our images indicating the shock wave position at different

times. Using filtering techniques on a computer program designed by us, we see 2 separate pictures for each frame captured by the camera.

We set up a system that used 2 different color dye lasers, shown in Figure 18. The Nd: YAG cavitation-inducing beam pumps both of the dye lasers which are optically delayed to two different times after the cavitations are induced. The Nd: YAG beam again has a frequency of 532 nm and a pulse duration of 2 ns. For this experiment the repetition rate of the Nd: YAG was 7.5 Hz because it was driven by the digital camera (see section 5.3). Both dye lasers have pulse durations of about 1 ns. The first dye laser is red (643 nm), and the second is light orange (583 nm—but it appears green on the camera). This results in images with two different rings in different colors, indicating the same shock wave at two different times.

A Nd: YAG laser passes through a partial reflector, as shown in Figure 18. The transmitted part induces cavitations, while the reflected part of the YAG beam passes through a second partial reflector. The reflected part of this beam pumps a first dye laser, and the transmitted part pumps a second dye laser. The two different color dye laser beams aim into the cuvette so that they pass through the region where the cavitations occur. After passing through the cuvette, the dye beams enter a microscope lens that images the cavitations onto a video camera. The difference in the path length of the Nd: YAG cavitation-inducing beam to the camera and the path lengths of the dye laser beams (each has a different path length) to the camera determines the delays after cavitation formation of the images seen.

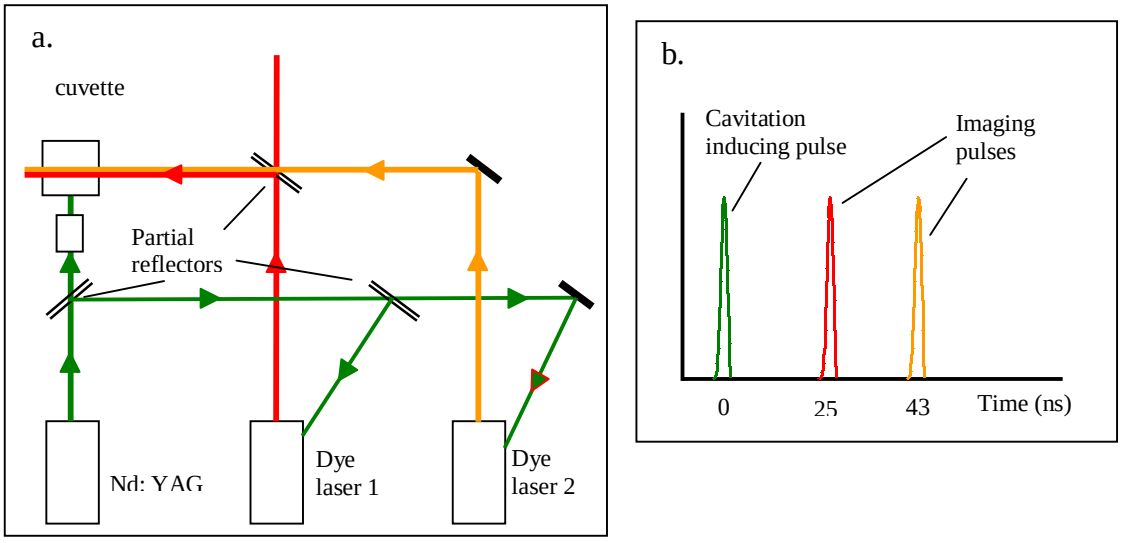

Figure 18 – Double optical delay with 2 dye lasers. (a) Setup. The YAG laser (green) passes into a partial reflector, which allows part of the beam to pass through to the cuvette to induce cavitations. The rest of the beam goes through another partial reflector. The reflected part pumps the first dye laser (red). The transmitted part pumps the second dye laser (light orange). The first dye laser passes into a partial reflector, and the reflected part of this dye beam passes through the cuvette to image the caviation. The second dye laser beam passes through this same partial reflector from the perpendicular direction, and the transmitted part goes into the cuvette to image the cavitation at a different time. (b) Relative delays. The delays of the imaging pulses are found by calculating their path difference from the starting point (the YAG laser) and dividing by the speed of light. The delays are also verified using an oscilloscope. Altering the beams' path lengths changes the delays.

Using a computer program of our design, we can eliminate red, green, blue, or any combination of them from the background of captured images. Therefore we can essentially obtain separate images for the different dye pulses, if they occur at different times as shown in Figure 19.

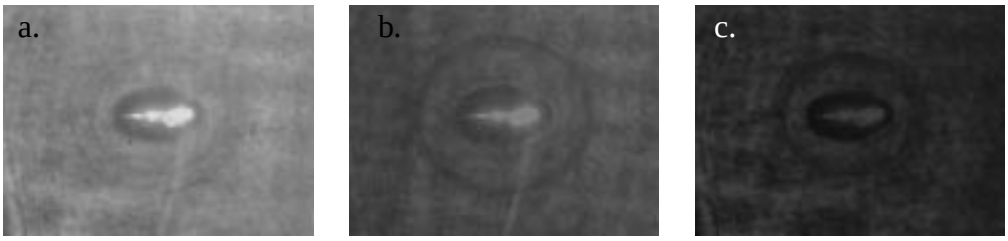

Figure 19 – Filtering Techniques. (a) The original, unfiltered image as captured by the camera. The image is composed of two dye laser pulses, one at 16 ns and the other at 24 ns. (b) Green Filter. Only the green parts of the image remain. It is very easy to clearly see the outline of the shock wave at 24 ns. (c) Red Filter. Only the red part remains. Now we have isolated the shock wave at 16 ns.

Once our images were captured and filtered, we measured the position of the top, left, right, and bottom edges for both of the shock waves. This was easily done because the computer program displays the vertical and horizontal pixels corresponding to the cursor position. Recently this process was simplified even more by allowing the user to simply click in a series of positions, and making the program record the vertical and horizontal pixel of each point. This information was loaded into Excel, where we then calculated the vertical and horizontal radius, center position, etc. of each shock wave. Knowing the time corresponding to each radius and the radii for gave us a description of the shock wave radius as a function of time. We could then obtain the velocity by curve fitting, using a model of our own design (described later). The velocity was then used to determine the shock wave pressure.

5.3 Digital Camera Setup

To obtain data more quickly we replaced our analogue camera with a color digital camera [8] (the analogue camera required us to go from camera to videotape and finally

onto the computer one frame at a time). The digital camera transmits data directly from the camera to the computer for analysis. In order to view cavitations, we had to time the camera's frame rate to coincide with the laser pulses. Otherwise, the camera may not be scanning for information on all parts of the screen when our imaging pulses occur. This means only part of a given cavitation appears on the camera.

To synchronize, we used the output from the V_{sync} pin on the camera to drive the laser pulses. The output from V_{sync} had to be run through a one shot circuit to make the pulse occur at the correct time and last for the appropriate duration to drive the laser. With this circuit in place, the Nd: YAG laser fires once for every frame on the camera (this turns out to be 7.5 Hz), at the correct time for us to be able to view cavitations. If the laser and camera are synchronized, the cavitations will occur completely on the screen. If not, a horizontal section of the image will be missing or the whole image will be blank. This results from the camera resetting at the wrong time, meaning part of the screen (or all of it) is off during the time when the imaging pulse reaches the camera.

5.4 Data and Analysis

As we found in our measurements of early times, there is considerable fluctuation in the shock wave radius for a given time, even under the same laser conditions (see Figure 20).

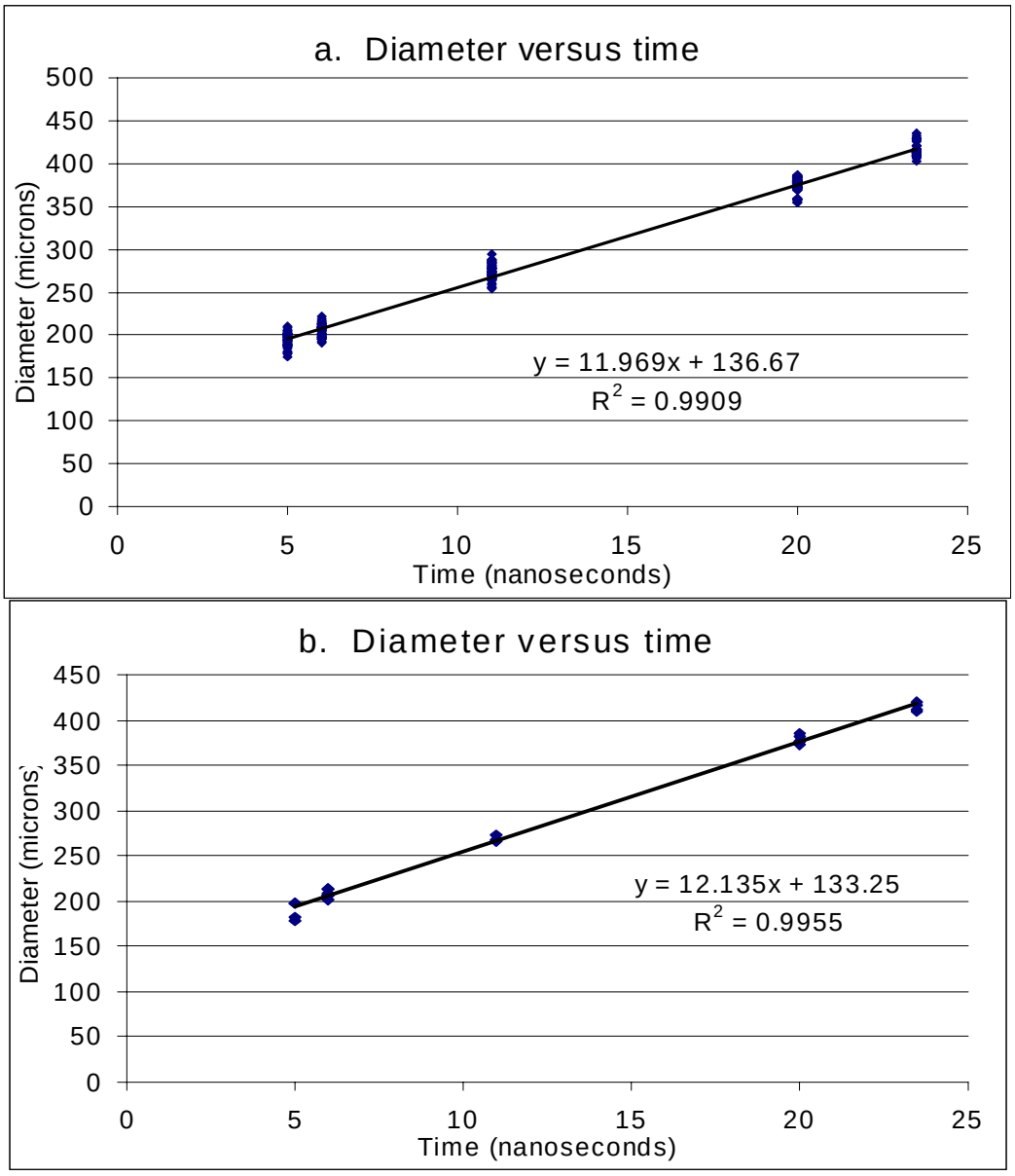

Figure 20 – Radius versus time. (a) Final radius not fixed. For a given time, the shock wave radius can vary by up to 50 microns. (b) Final radius fixed. For a given time, the shock wave velocity is more consistent.

In Figure 21, we plot the diameter at a variable time against the diameter at 16 ns.

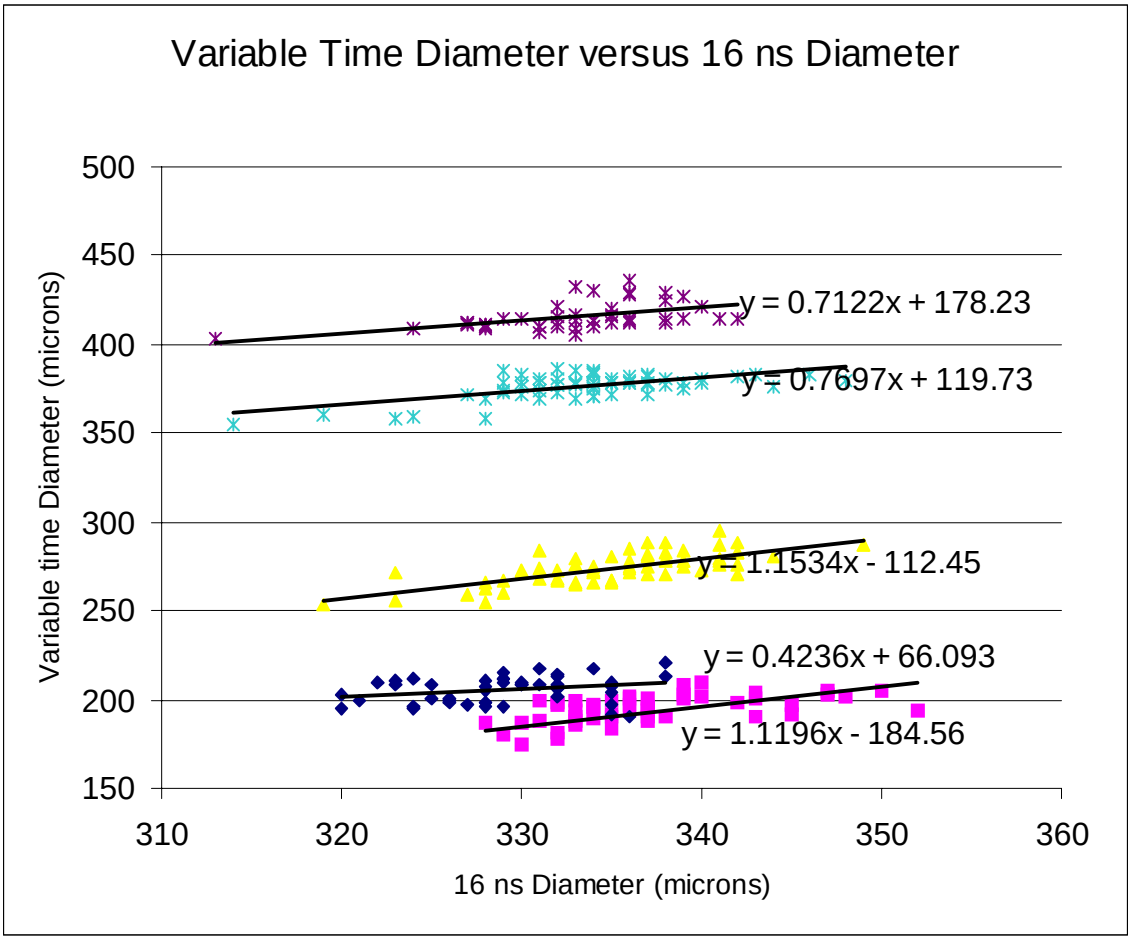

Figure 21 – Variable shock wave diameter versus the 16 nanosecond diameter for all data. Different colored groups correspond to different variable time delays. Lines that are higher on the graph correspond to a later time for the variable shock wave diameter measurement. In all analysis from here on, we chose points that lie on a vertical line in this graph in order to have reliable results.

For a fixed 16 ns radius (Figure 22), the curve for radius versus time fits a nice curve. In our analysis we treated these points as if they were from the same cavitation.

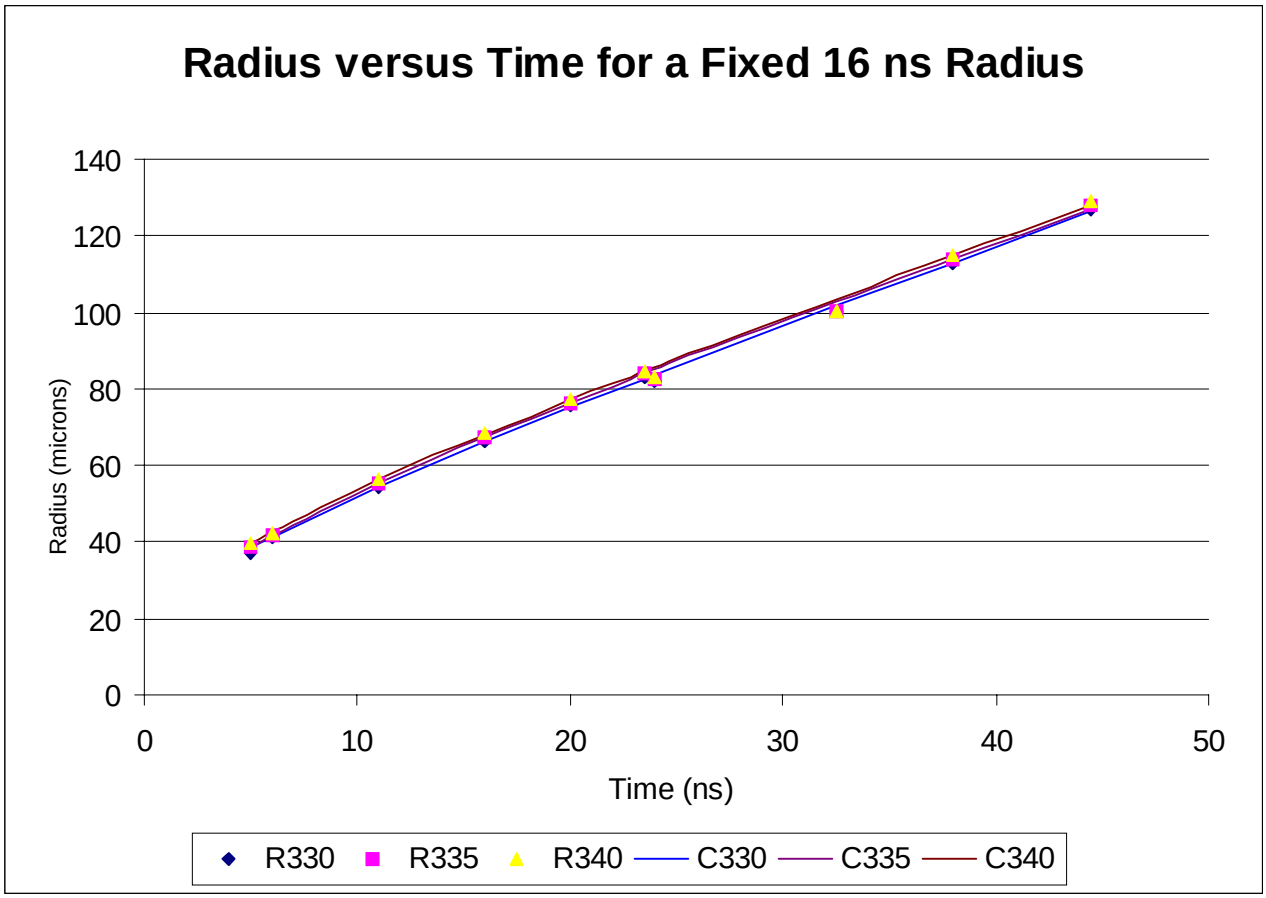

Figure 22 – The shock wave radius versus time for a fixed 16 nanosecond radius (raw data). Data sets from different 16 ns radii are given at the bottom (For example, R330 corresponds to a radius of 330 microns at 16 ns.) The lines are curve fits.

We obtained this data using a light orange dye laser and a red dye laser with different optical delays. For all runs, we fixed the red dye laser at a 16 ns delay, while we varied the red dye laser delay from 5, 6, 11, 20, 23.5, 24, 32.5, 38, and 44.5 ns. As done in the 1-30 microsecond studies, we selectively grouped our data by fixing one of the pulses and varying the other. To get an accurate description of pressure evolution, we only

compared shock waves with the same radius at 16 ns. Using this technique, we can treat shock waves from different cavitations as the same shock wave. Because this data was taken on two separate occasions (one group was 5-23.5 ns and the other was 24-44.5 ns) we also compared the shock wave radii from 23.5 ns to the radii from 24 ns in a similar fashion.

The result of these techniques is a description of the shock wave radius of essentially the same cavitation at times of 5, 6, 11, 16, 23.5, 24, 32.5, 38, and 44.5 ns after the initial cavitation formation. Using the equations mentioned in the theory, we created a model for the radius as a function of time. From this we found the velocity and pressure as a function of time. For the shock wave energy to be constant,

$$R_m(p_s - p_\infty) = F \tag{10}$$

where R_m is the shock wave radius, p_∞ is 1 atm, and F is a constant. From the model equations, we also know that pressure varies linearly with velocity. That is

$$(p_s - p_\infty) = A(u_s - c_0) \tag{11}$$

where A is a constant, and we compare the pressure above atmospheric pressure to the shock wave velocity above the speed of sound. Combining these two equations we find

$$AR_m(u_s - c_0) = F \tag{12}$$

If we integrate this equation with respect to time, we can find the radius as a function of time

$$c_0 t = R_m - r_0 \ln(1 + R_m / r_0) \tag{13}$$

where

$$r_0 = \frac{F}{A c_0} \tag{14}$$

is a characteristic radius. It can be shown that r_0 is the radius at which the shock wave velocity is twice the speed of sound in the liquid.

We can use this model to curve fit our data, using the solver function in Excel (see Figure 23). This model predicts a final velocity of 1500 m/s, which is in agreement with the expected value of 1483 m/s. In this model, we have allowed the shock wave radius to start at a value greater than zero. This takes into account that the cavitation may start at the top of the beam waist (the cavitation is displaced by the spot size length from the origin).

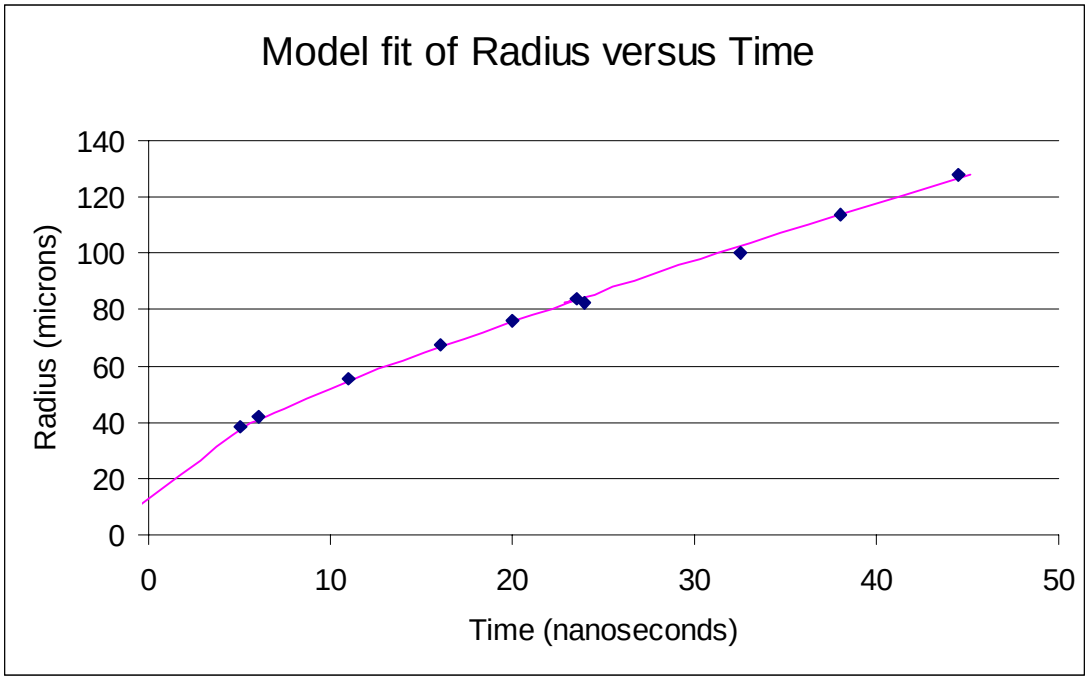

Figure 23 – Model fit of our data for radius versus time. The model is based on the derivation above. Using the solver function in Excel, we minimize the error in the function (error between the model values compared to our values) by adjusting the parameters for r_0 (which are E_s, c_0, and A, the constant to convert velocity to pressure based on the Taylor's series expansion). The final velocity is predicted to be 1500 m/s.

To obtain velocities, we differentiate equation (13) with respect to time, and obtain the shock wave velocity as a function of radius, which can then be used to find the velocity as a function of time. The result is shown in Figure 24.

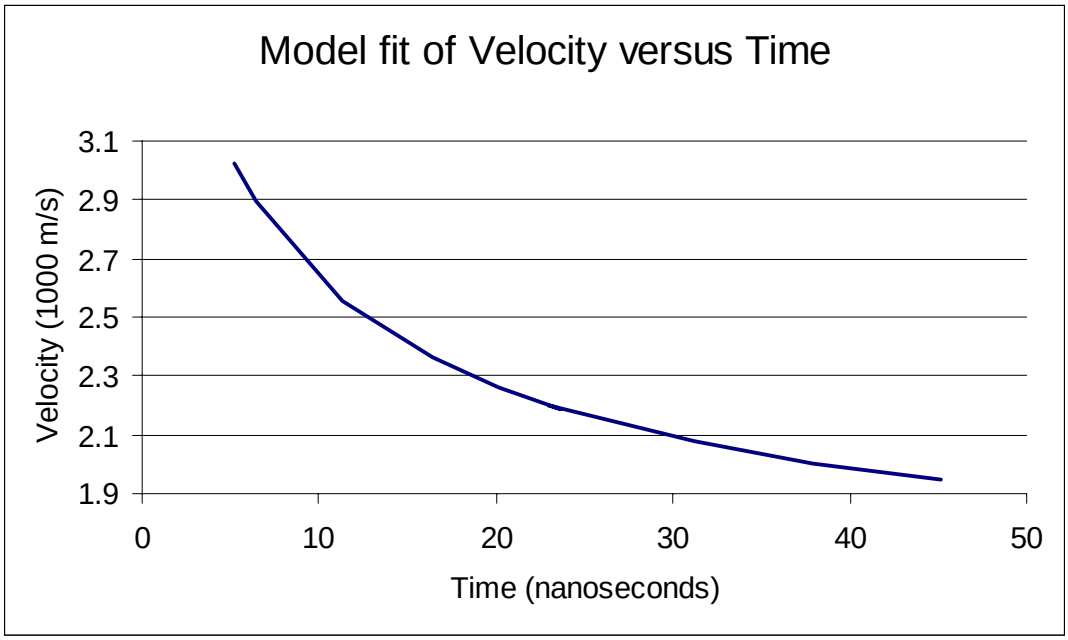

Figure 24 – Model fit of velocity versus time. Using our model, we can find the velocity versus time from the slope of the radius versus time graph. The model predicts a maximum velocity of nearly 3100 m/s at 5.2 ns after the cavitation is formed. At 45 ns, the shock wave velocity is still far from its minimal value of 1500 m/s.

To obtain a pressure from these velocities, we simply insert these velocity values into the equations (8) and (9). The resulting values are plotted in Figure 25. We also plot pressure as a function of radius in Figure 26.

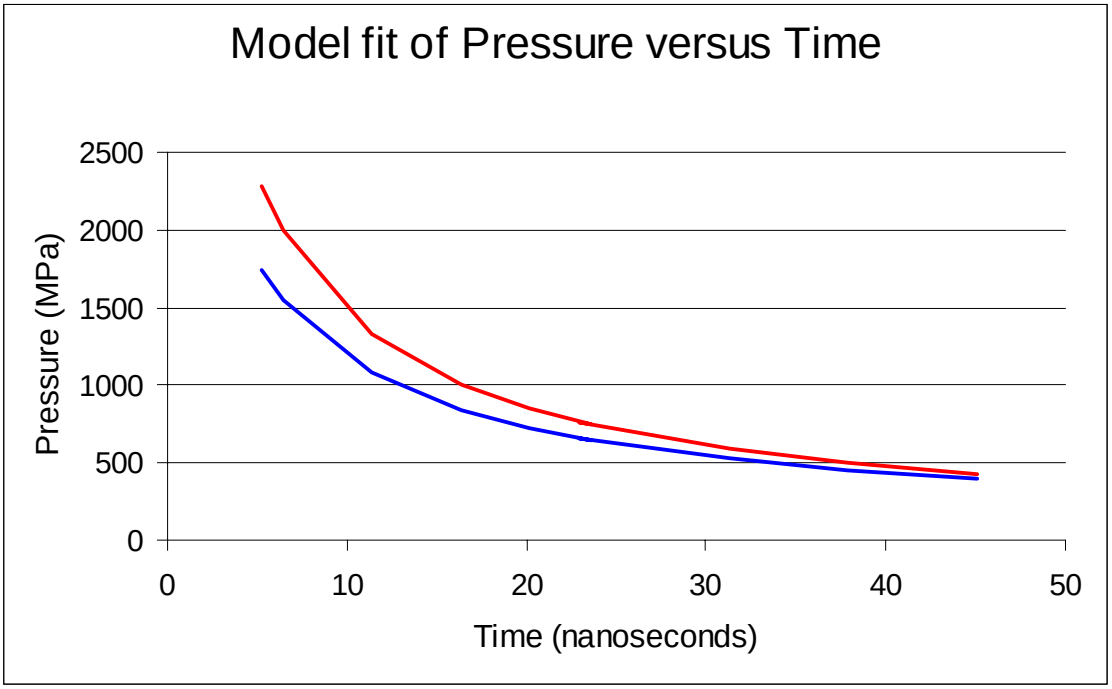

Figure 25 – Model fit of pressure versus time for the Rice and Walsh model (red) and the Tait equation (blue). The maximum pressure is in the range of 1700 to 2300 MPa at 5.2 nanoseconds.

The pressures our model predicts are enormous. The maximum pressure is 2300 MPa (about 23000 atm—that is 23000 times atmospheric pressure) according to the Rice and Walsh model, or 1700 MPa according to the Tait equation at 5.2 ns, and 38.4 microns. There is some question as to the validity of our model for the radius as a function of time. Close inspection of the data points show that they fit a linear model very well (Figure 27). However, this leads to a problem because it results in a constant velocity of 2200 m/s, which is far from the expected final velocity of 1483 m/s. Also this predicts the shock wave to begin at 29 microns from the origin, which is also not possible.

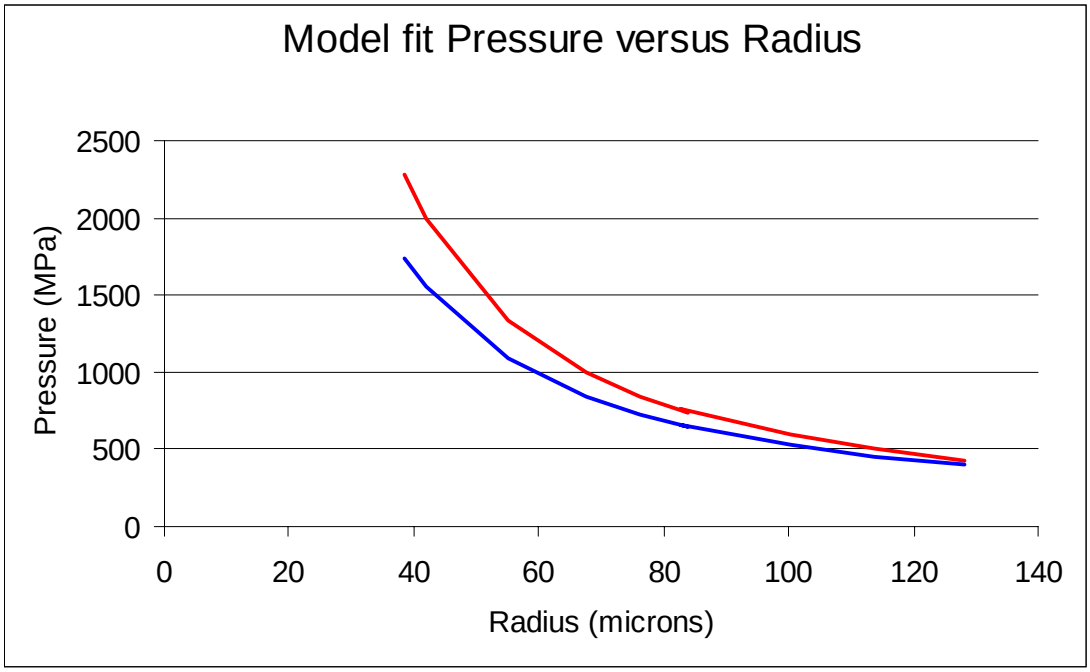

Figure 26 – Model fit of pressure versus radius. The Rice and Walsh model predicts the red curve and the Tait equation predicts the blue curve. The maximum pressure occurs at the shortest radius.

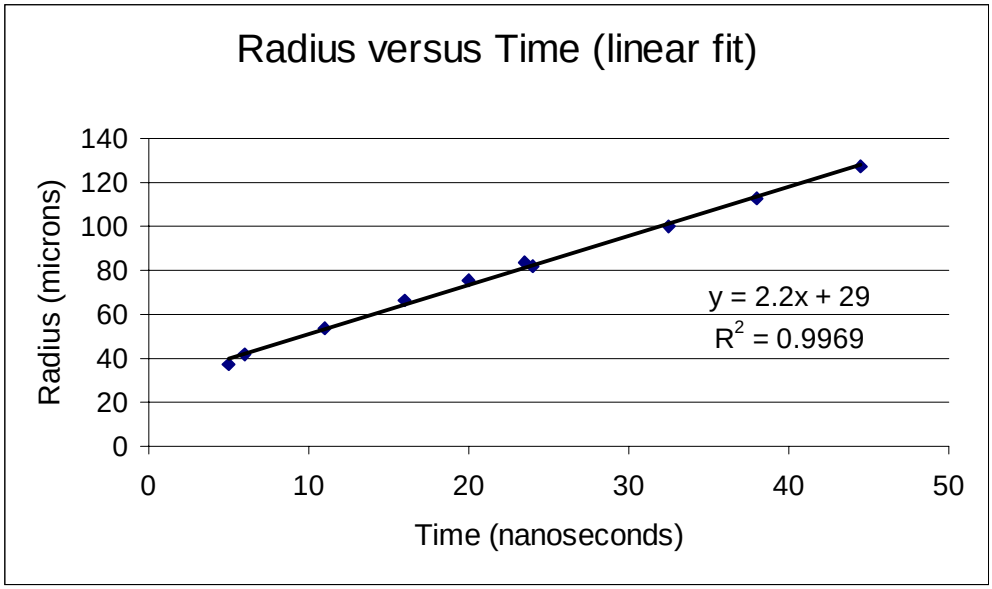

Figure 27 – Radius versus time with a linear fit. The raw data points fit a linear curve very well. This model predicts a constant shock wave velocity of 2200 m/s. We expect the shock wave velocity to dissipate to 1483 m/s, so this would have to result from a huge calibration error.

Possible reasons for error in these calculations is the varying laser energies used for our data set. For example, for the data taken at 5 and 16 ns, the laser energy was 772 microjoules, while the energy for the 16 and 24 ns data was 434 microjoules. Despite our best efforts to group similar cavitations, these energy differences are likely to cause problems. Unfortunately this is a difficult problem to avoid because the output power of our Nd: YAG laser varies tremendously depending on how long it has been running.

If the shock wave velocity is in fact a constant value of 2200 m/s, it is an error of roughly 48 percent. This could only be partially due to a problem with calibration leading to radius measurement errors. Another possibility is that the 10 micron polystyrene spheres contained in the liquid could change the speed of sound of the liquid. Further studies must be done to find the cause of this possible discrepancy (this is only a problem if we do not believe or model). We can test this by looking at even longer delays to see if the data points fit our present model fit. In these studies we will also attempt to keep the laser power more consistent by monitoring it closely, and leaving the laser on longer before beginning to take data.

Regardless of the cause of this possible error, our pressure calculations will subsequently be affected by it. Plotting the shock wave energy versus time is one way to determine if this error is real. Using an equation, we can determine the energy associated with this pressure. The energy for a shock wave is given by

$$E_s = \frac{4\pi R_m^2}{\rho_0 c_0} \int p_s^2 dt \tag{15}$$

Where R_m is the distance from the emission center, ρ_0=1000 kg/m^3, c_0 is the speed of sound (1483 m/s), and p_s is the pressure [9]. Instead of using the time integral, we can

transform the $4\pi R_m^2$ into the volume of the shock wave, where we take into account the width of the shock wave. This results in the equation

$$E_s = \frac{V_{shell}}{\rho_0 c_0 u_s} p_s^2 \tag{16}$$

where V_{shell} is the shell volume. The results of this calculation are shown in Figure 28 for both pressure models.

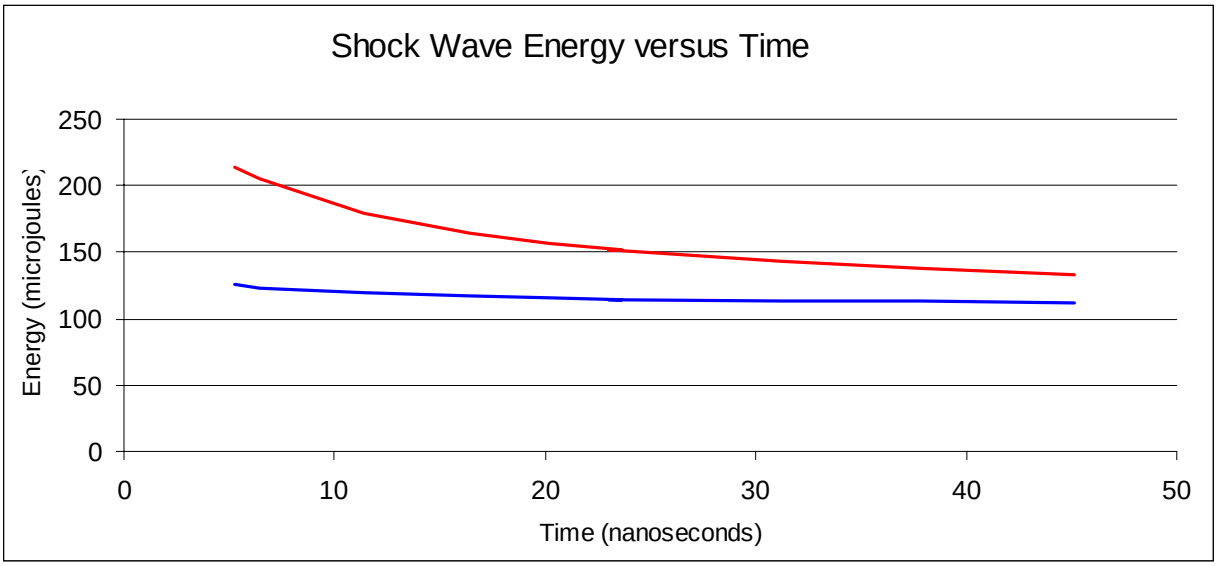

Figure 28 – Model fit of shock wave energy versus time. The Rice and Walsh model predicts the red curve, and the Tait equation predicts the blue curve. We expect the shock wave energy to be constant. Therefore we will use the Tait equation in our evaluation of pressure values.

The shock wave energy is roughly 125 microjoules using the Tait equation. If we compare this to the laser energy of 772 microjoules, we see that about 16% of the laser energy is converted to shock wave energy. The Rice and Walsh model predicts that about 25% of the laser energy is converted to shock wave energy. Previous studies

indicate that for a 6 ns, 1 mJ pulse, the 36.4% of the laser energy goes to the shock wave, and that this energy decreases for shorter pulses and lower energies [3]. The fact that the energy curve is nearly flat based on the Tait equation indicates that the Tait equation agrees more closely with our linear model (13). This makes sense because the quadratic term in the Taylor expansion of the Tait equation (8) is smaller than that of the Rice and Walsh Taylor expansion (9). Also, although the pressures predicted by our model are very large, they are in fact consistent with results of others.

Other sources have found maximum pressures of 8803 MPa, for a 6 ns, 10 mJ laser pulse, and a 7 micron spot size [4]. Since our laser pulse was 2 ns, laser energy was 772 microjoules, and spot size was 10 microns, it is reasonable that our maximum pressure is considerably smaller.

6. Conclusions

Results obtained from our color digital camera setup indicate that the speed of the shock waves at early times (5 ns to 45 ns) are well above the speed of sound in water, allowing us to use equations (6) and (7) in our analysis of pressures. We found that the pressures are immense. The maximum pressure occurred at the earliest times studied, and using the Tait equation, we found this to be 1700 MPa (about 17000 atm,17 kilobars, or 17 metric tons per cm^2) at 5.2 ns, and 38.4 microns. This is equivalent to a sound level of 240 decibels (a nuclear explosion at 500 m is 220 decibels). The Rice and Walsh equation predicts even higher pressures. Although the pressure is tremendous, we find that it is in qualitative agreement with other studies [4]. After very early times, the bubble grows inertially and has moderate pressure at microsecond times. The maximum

pressure found for times 1 to 30 microseconds was only about 2.5 atmospheres at 2 microseconds.

We question the validity of our model fit based on equation (13) because the radius appears to vary linearly with time. However, we believe this could be due to an error in our matching of data sets, but is more likely due to the lack of data points at later times. To investigate this possible error, we will take more data using a constant laser energy and investigate the shock wave radius at later times.

Our count rate data is for the most part consistent with our expectations (given in Section 3.1). However, our results have shown us that the number of explosions per unit time depends on unexpected factors (particularly in water). Apparently the count rate depends on time after initial placement in beam (in water) and on the exact placement of the cuvette.

There are still many things we need to do before this project will be complete. After we obtain an accurate pressure description, the next step is to set up a system under a microscope to use the shock waves in applications. We hope to eventually be able to use these cavitations in biological applications. One idea has been to use the cavitations to fuse liposomes together. Studies have been done using lasers to pierce lipid vesicles to remove objects inside them [10] while leaving the vesicle unharmed, so fusing liposomes together may be possible as well. Another idea has been the possibility of injecting chemicals into cells using cavitation pressures. Both of these phenomena would have important biological applications. Eventually we will set up a system under the microscope in which we can induce a single cavitation to do one of these tasks.

References

[1] C.D. Ohl, O.Lindau, Lauterborn, “Luminescence from Spherically and Aspherically Collapsing Laser Induced Bubbles”, *Phys. Rev. Lett.* **80** 393-397, (1998).

[2] A. Philipp, W. Lauterborn, “Cavitation Erosion by Single Laser-Produced Bubbles”, *J. Fluid Mech.* **361**, 75 - 116 (1998).

[3] A. Vogel, J. Noack, K. Nahen, D. Theisen, S. Busch, U. Parlitz, D. X. Hammer, G. D. Noojin, B. A. Rockwell, and R. Birngruber, "Energy balance of optical breakdown in water at nanosecond to femtosecond time scales," *Appl. Phys. B* **68**, 271 (1999).

[4] A. Vogel, S. Busch, and U. Parlitz, "Shock wave emission and cavitation bubble generation by picosecond and nanosecond optical breakdown in water," *J. Acoust. Soc. Amer.* **100**, 148 (1996).

[5] B. Jacobs and W. E. Cooke (private comm. 2003)

[6] I. Larina, C. Bartels, K. Larin, R. Esenaliev, “Cavitation-induced drug delivery in tumors for cancer chemotherapy: phantom studies,” *SPIE-Int. Soc. Opt. Eng. Proceedings of Spie – the International Society for Optical Engineering*, vol. 4257, 385-92, (2001).

[7] J. M. Richardson, A B. Arons, and R. R. Halverson, “Hydrodynamic Properties of Sea Water at the Front of a Shock Wave,” *J. Chem. Phys.* **15**, 785-795, (1947).

[8] The purchase of this camera was made possible by a Howard Hughs Medical Institute Grant through the Undergraduate Biological Sciences Education Program to the College of William and Mary.

[9] R.H. Cole, *Underwater Explosions* (Princeton U.P., Princeton, NJ, 1948).

[10] J. David Moroz, Philip Nelson, Roy Bar-Ziv and Elisha Moses, "Spontaneous Expulsion of Giant Lipid Vesicles Induced by Laser Tweezers," *Phys. Rev. Lett.* **78** (1997) 386.

[11] B.J. Schwartz and P.J. Rossky, "Pump-Probe Spectroscopy of the Hydrated Electron: A Quantum Molecular Dynamics Simulation," *J. Chem. Phys.* **101**, 6917 (1994).